Jurnal Teknologi, 43(D) Dis. 2005: 45–60

INTEGRATION OF FINGERPRINT CENTRE POINT LOCATION AND PRINCIPAL COMPONENT ANALYSIS FOR FINGERPRINT VERIFICATION

CHAN YING HUI[1] & SYED ABDUL RAHMAN ABU BAKAR[2]

Abstract. This paper presents an efficient algorithm for estimating the location of the centre point (CP) of a fingerprint for the purpose of aligning fingerprints in a fingerprint verification system. Principal Component Analysis (PCA) is utilized in this system. The proposed CP estimation algorithm is based on the Alteration Tracking (AT) followed by an estimation algorithm. AT is proposed to extract a track that records the transition from one quantized direction to another while the Centre Point Estimation (CPE) algorithm is used to find the bending point with highest direction transition from the transition track. Fingerprint feature extraction is obtained with respect to the CP of the fingerprint directional field. PCA is then performed over the centred fingerprint directional field to extract important information from fingerprint features for verification purpose. Experimental result shows that the proposed CP algorithm is capable of reliably aligning fingerprints. Furthermore, PCA is able to extract information from aligned fingerprint directional field for fingerprint verification.

Keywords: Biometrics, fingerprints, fingerprint centre point, fingerprint verification, PCA

Abstrak. Dikemukakan algoritma menentukan pusat cap jari untuk menjajar cap jari dalam sistem pemeriksaan cap jari. Analisis Komponen Prinsipal (PCA) digunakan dalam sistem ini. Algoritma menentukan pusat cap jari dicadangkan dengan menggunakan Jejak Ubahan diikuti dengan Penaksiran Pusat Cap Jari. Jejak Ubahan dicadangkan untuk mendapatkan trek yang merekod peralihan arah manakala Penaksiran Pusat Cap Jari bertujuan untuk mencari titik semasa trek membengkok yang mempunyai peralihan arah yang paling ketara. Maklumat cap jari diperoleh berdasarkan pusat cap jari yang telah ditentukan daripada imej berarah cap jari. Proses PCA dilaksanakan terhadap maklumat imej berarah cap jari untuk mendapatkan maklumat penting daripada maklumat cap jari bagi menjalani pemeriksaan cap jari. Keputusan eksperimen menunjukkan bahawa algoritma yang dicadangkan berupaya untuk menjajar cap jari. Tambahan pula, PCA berkemampuan untuk memperoleh maklumat daripada imej berarah cap jari yang tersusun untuk menjalani pemeriksaan cap jari.

Kata kunci: Biometrik, cap jari, pusat cap jari, pemeriksaan cap jari, PCA

1.0 INTRODUCTION

The directional field of a fingerprint is defined as the local orientation of the ridge-valley structures, describing the coarse structure or basic shape of a fingerprint [1]. It is widely used in fingerprint registration or reference point location, classification and

[1&2] Department of Microelectronics and Computer Engineering, Faculty of Electrical Engineering, Universiti Teknologi Malaysia, 81310 Skudai, Johor, Malaysia. Tel.: 07-5535238.
Email: [1]yuichan@yahoo.com, [2]syed@fke.utm.my

matching. Reference point location algorithm presented in [2] calculates the difference of sine component for orientation field between adjacent regions.

Automatic fingerprint recognition systems are often faced with the problem of fingerprint translation during the acquisition. Centre point (CP) location is therefore, an essential first step for fingerprint alignment. Most of the available algorithms for locating the CP are by finding a core point from the directional field of a fingerprint based on Poincaré index, for example in [3] and [4]. However, Poincaré index is able to locate singular points, thus problem arises for arch type fingerprints.

As for the fingerprint analysis, Principal Component Analysis (PCA) seems to be the method of choice. A PCA-based method is proposed in the estimation of a high resolution directional field for fingerprints by computing a direction in every pixel location [5]. PCA is applied to an autocovariance matrix obtained from gradient vectors, thus providing a 2-dimensional Gaussian joint probability density function of the vectors. The gradient orientation corresponds to the longest axis of the Gaussian joint probability density function that belongs to the largest eigenvalue. As the ridge-valley orientations are perpendicular to the gradient orientation, it corresponds to the shortest axis of the Gaussian joint probability density function that belongs to the smallest eigenvalue.

2.0 FINGERPRINT VERIFICATION SYSTEM OVERVIEW

Figure 1 illustrates an overview of the different modules that constitute a fingerprint verification system.

Figure 1 Fingerprint verification flow diagram

An input fingerprint image captured using a fingerprint sensor is directed to the fingerprint CP location module. This is a crucial step for achieving a consistently aligned image so that fingerprint registration procedure would be avoided and hence, enabling the system to perform fast verification process in real-time. The proposed fingerprint feature extraction is performed based on the result of fingerprint CP location module. PCA, which encodes information in a sense of compressing, is employed for training enrolled features and recognizing query features during verification stage. Similarity measures are applied in the final stage to determine whether the claimed identity could be verified or not. Similarity measures employed include the Euclidean distance (ED) and the Mahalanobis distance (MD) measurements.

3.0 FINGERPRINT CENTRE POINT LOCATION

In this paper, the CP is defined as the point of maximum curvature of the concave ridges in a fingerprint [2]. Most of the available algorithms search for the CP from every single pixel in the fingerprint directional image. An alteration track is used to obtain a quick CP location by considering a small window of neighbouring pixels along the track. We first construct a fingerprint directional field. We then perform a grayscale opening operation followed by Alteration Tracking (AT) and the CP Estimation (CPE) operations.

During the discussion, the following notations will be used. Let N be the size of the captured input fingerprint, M and P are illustrated in Figure 3, and Q denotes the total number of CP candidates for type 1 and type 2. The values are: $N = 416$, $M = 30$, $P = 22$, $Q = 10$, and $P < M$. These parameters except N are determined from empirical experiments. The values of the four parameters are applied for the rest of this paper.

3.1 Fingerprint Directional Field Construction

The fingerprint directional field used in this paper is obtained from the work carried out by [6]. Let the original input fingerprint be $N \times N$ in dimension and $W^2_{\text{vert}}(i, j)$ and $W^2_{\text{hori}}(i, j)$ denote the vertical and horizontal details of the second stage wavelet transform images respectively. Ridge orientation estimation is computed using Equation (1):

$$\theta_{(i,j)} = \tan^{-1}\left[\frac{W^2{}_{vert}(i,j)}{W^2{}_{hori}(i,j)}\right] \tag{1}$$

where $i = 0, 1, 2, \ldots, N/4 - 1$, $j = 0, 1, 2, \ldots, N/4 - 1$. We then obtained the directional field by quantizing the ridge orientation into eight directions as tabulated in Table 1 and smoothing it using a 7×7 smoothing filter before down sampling it by a factor of two. Quantized value is obtained as the middle value within orientation range. The resultant directional field image size thus is $N/8 \times N/8$.

Table 1 Eight directions quantization

Range of θ (°)	Quantized value of θ (°)	Grayscale representation
$-90.0 < \theta \leq -67.5$	–78.75	0
$-67.5 < \theta \leq -45.0$	–56.25	36
$-45.0 < \theta \leq -22.5$	–33.75	72
$-22.5 < \theta \leq 0.0$	–11.25	108
$0 < \theta \leq +22.5$	+11.25	144
$+22.5 < \theta \leq +45.0$	+33.75	180
$+45.0 < \theta \leq +67.5$	+56.25	216
$+67.5 < \theta < +90.0$	+78.75	252

3.2 Grayscale Opening Operation

Grayscale opening is a morphological operation that involves two successive basic operations: grayscale erosion followed by grayscale dilation. We employed grayscale opening operation over the grayscale representation of directional field obtained from Section 3.1 in order to smooth the transition edge between grayscale value 144 representing +11.25° and grayscale value 108 representing –11.25°. At the same time, this operation will also eliminate grayscale values representing large degree of angle (brighter pixels) within region of grayscale values representing small degree of angle (darker pixels). We used a 3×3 structuring element as a convolution mask. Figure 2 illustrates an example of the original, fingerprint directional field and opened fingerprint directional field in eight quantized grayscale representation.

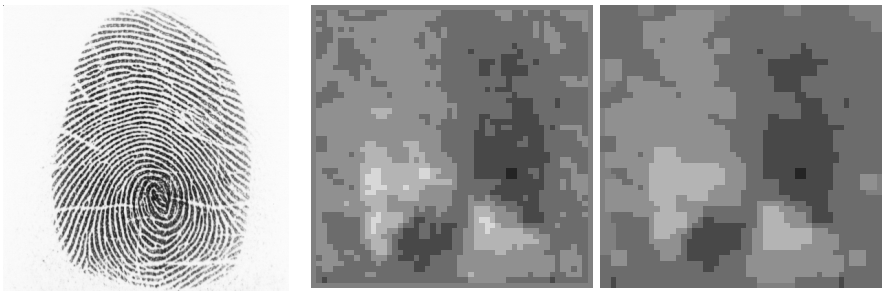

(a) (b) (c)

Figure 2 An example of (a) fingerprint, (b) directional field, (c) opened directional field

3.3 Alteration Tracking

We searched for the AT within a region of $M \times M$ pixels from the centre of $N/8 \times N/8$ pixels of the opened fingerprint directional field. This is to ensure that there will be enough alteration pixels for recording transition between the two different orientation values represented by different gray values (see Table 1). Alteration track region is only valid within region of interest (ROI) $P \times P$ pixels surrounding the centre of the opened fingerprint directional field. The reason is to ensure that the cropped fingerprint directional field of size $N/16 \times N/16$ consists of informative region. This will be explained in Section 4. The highlighted region in Figure 3 is the ROI.

A middle alteration track records the transition from pixel value 144 to pixel value 108. We chose to set the middle track pixel value to 108 due to the fact that there is no grayscale value representing 0°. We started by performing the Left Chain Code (LCC) mechanism with initial condition model (shown in Figure 4(c)). If the track is broken and the LCC with alteration track pixel model is not able to acquire a track pixel, we applied a continuous initial condition LCC model (Figure 4(b)) to obtain another starting point.

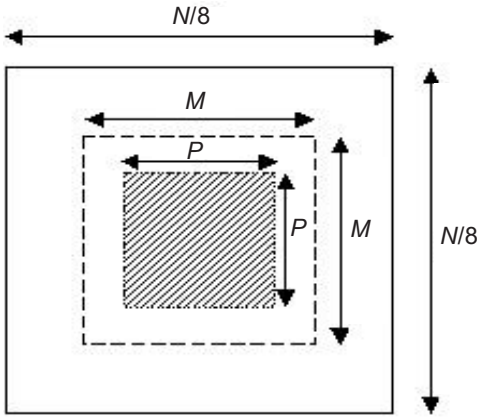

Figure 3 Region of interest

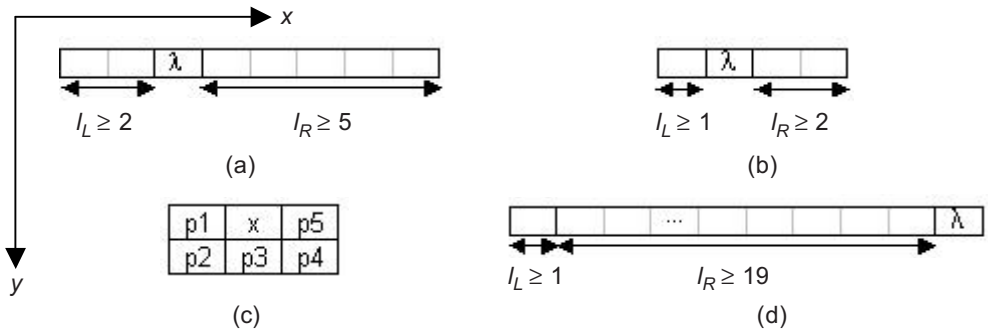

Figure 4 Middle alteration tracking (a) initial condition for LCC, (b) continuous initial condition for LCC, (c) LCC and (d) middle alteration track model

As shown in Figure 4, λ pixels are the locations of the candidate track pixels with value of 108. The initial condition in Figure 4(a) shows that if there are at least 2 pixels ($l_L \geq 2$) to the left of the candidate pixel having grayscale value 144 and at least 5 pixels ($l_R \geq 5$) to the right of the candidate pixel having grayscale value ≤108, then the candidate pixel is a valid starting pixel for the alteration track. The same case applies to the continuous initial condition in Figure 4(b) with a modification; $l_L \geq 1$ and $l_R \geq 2$. The continuous starting pixel is valid alteration track pixel only if the absolute difference of the x-coordinate between the last alteration track pixel and the continuous starting pixel is less than $M/2$ pixels. This last value was determined empirically. In Figure 4(c), '*x*' is the origin of LCC representing position (x, y). The highest priority is given to *p1* with the highest priority, followed by *p2*, *p3*, *p4* and *p5* in an anticlockwise manner. Then, placed the middle alteration track model shown in Figure 4(d) at position *p1*, *p2, p3, p4* and *p5* accordingly to determine which pixel is the next valid track pixel.

The selected pixel is a valid alteration track pixel if $l_L \geq 1$ having grayscale value of 144, and $l_R \leq 19$ having grayscale value of 108. In case of *p1* and *p5*, there are additional conditions need to be satisfied before either one of them could be a valid track pixel, i.e. *p1* must reside between regions with grayscale value ≥144 at location (x-1,y-1) and grayscale value ≤108 at location (x-1,y+1). Similarly, *p5* must reside between regions with grayscale value ≤108 at location (x+1,y-1) and grayscale value ≥144 at location (x+1,y+1). Experimentally, three types of middle alteration track have been obtained, as shown in Figure 5 viz: (a) whorl fingerprints fall into either one of type 1 or 2, (b) right loop has type 1 alteration track, (c) left loop has type 2 alteration track, (d) type 3 represents a nearly straight line that applies to arch and tented arch fingerprints.

Figure 5 Middle alteration track for (a) type 1, (b) type 2 and (c) type 3

3.4 Centre Point Estimation

Centre Point Estimation (CPE) is aimed at finding the location with maximum bending point along the middle alteration track for type 1 and 2. For type 3, CPE will utilize not only the middle alteration track but also the left and right alteration tracks. This will be discussed towards the end of this section. It is imperative to note that CPs for type 1, 2 and 3 can be detected only if they are within the ROI. A precise track is the key to successfully estimate an accurate CP. In searching for the CP, we first assumed the alteration track is of type 1. We then applied the type 1 search model. If the search fails, we proceed with type 2 search. If this stage also fails, we then apply the type 3 search.

Figure 6 illustrates scanning method, center point model and noise elimination method for both type 1 and 2. Let λ be a CP candidate pixel. Similarly, let *Nw* (northwest), *Ne* (northeast), *Sw* (southwest) and *Se* (southeast) be pixels used for type 1 and 2 CP models, and γ be the noise pixel. Note that the scanning direction for type 1 is from bottom to top and right to left (BTRL), as shown in Figure 6(a). The search for type 1 CP candidates (the maximum number of CP candidates while sliding the type 1 CP model is *Q2*) can be summarized in the following steps.

Step 1: Slide type 1 model in the direction given above with λ on the middle alteration track.

Step 2: Examine whether *Nw, Ne* and *Sw* pixels on the type 1 CP model obey dominant grayscale values. These are given as below:

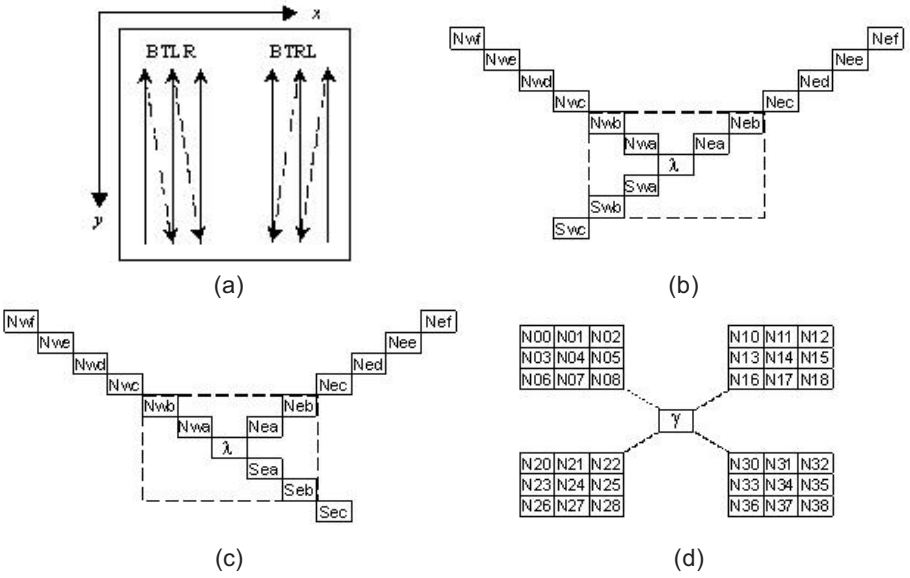

Figure 6 (a) scanning method, (b) type 1 centre point model, (c) type 2 centre point model and (d) noise elimination method

dominant grayscale value for *Nw* ≥144,
dominant grayscale value for *Ne* and *Sw* ≤108.

Step 3: if *Nw, Ne, Sw* or *Se* is within dotted bounding box then,
the pixel must obey dominant grayscale values
else
Examine the pixel by using noise elimination method to determine whether it is a noise
end if

Step 4: Repeat step 1 until the maximum number of type 1 CP candidates is achieved or when there is no more track pixel.

Noise elimination method is explained through the following examples. Suppose the pixel that does not obey the dominant grayscale value is *Nwc*, then consider *Nwc* to be γ in Figure 6(d). At first look into a pixel which is in same direction at location *N04*, which is at 6 pixels offset in both x- and y-coordinates from γ, and a pixel in the perpendicular directions at location *N14* and *N24*, which are at 3 pixels offset in both x- and y-coordinates from γ. The rule is that if more than 3 neighbours from the 3×3 neighbourhood centred at *N04*, and either of the two 3×3 neighbourhoods centred at *N14* or at *N24* obey the dominant grayscale value, then *Nwc* is considered as a noise pixel and is assigned to the marginally dominant grayscale value, i.e. 144 in this

case. Suppose the noise pixel is *Ned*, then it is assigned to its marginally dominant grayscale value, i.e. 108. Two average values for pixels of dominant grayscale ≥144 and ≤108 are calculated for each CP candidate. Pixels with grayscale value >180 is set to 180 and pixels with grayscale value <72 is set to 72. From our observation, these 4 grayscale values (180, 144, 108 and 72) are able to provide essential information to locate a true CP while additional gray level values will bias the result.

The search for type 2 CPE is very much similar to the search for type 1 CPE except that scanning is now conducted from bottom to top and left to right (BTLR) as shown in Figure 6(a) and the dominant grayscale value for southeast (*Se*) is ≥144. Note that the maximum number of CP candidates while sliding the type 2 CP model is $Q/2$.

The value of Q, which is determined empirically, must not exceed 10. We then calculate the following statistical values which can be summarized as the following:

$$domgrayL_i = \begin{cases} \dfrac{Nwa + Nwb + Nwc + Nwd + Nwe + Nwf}{6} & 0 \le i \le \frac{Q}{2} - 1 \\ \dfrac{Nwa + Nwb + Nwc + Nwd + Nwe + Nwf + Sea + Seb + Sec}{9} & \frac{Q}{2} \le i \le Q - 1 \end{cases} \tag{2}$$

$$domgrayR_i = \begin{cases} \dfrac{Nea + Neb + Nec + Ned + Nee + Nef + Swa + Swb + Swc}{9} & 0 \le i \le \frac{Q}{2} - 1 \\ \dfrac{Nea + Neb + Nec + Ned + Nee + Nef}{6} & \frac{Q}{2} \le i \le Q - 1 \end{cases} \tag{3}$$

$$diffL_i = domgrayL_i - \underset{i}{Max}(domgrayL)\Big| \qquad i = 0, \ldots, Q-1 \tag{4}$$

$$diffR_i = domgrayR_i - \underset{i}{Min}(domgrayR)\Big| \qquad i = 0, \ldots, Q-1 \tag{5}$$

$$score_i = diffL_i + diffR_i \tag{6}$$

where *domgrayL* and *domgrayR* are the average dominant grayscale value ≥144 and dominant grayscale value ≤108 for type 1 and 2, respectively. The absolute difference between i^{th} *domgrayL* and the maximum value among Q CP candidates is indicated by *diffL*; the absolute difference between i^{th} *domgrayR* and the minimum value among CP candidates is represented by $diffR_i$. The final decision for the above statistical analysis is given by $score_i$, which is the likelihood measure of i^{th} CP candidate for not being a true CP. A CP candidate with the lowest score will be the winner and it will be chosen as the true CP.

If there is no CP found from the above algorithm, it is possible that the track is not a typical type 1 or type 2, but a variant of them. An example of a variant for type 1 is demonstrated in Figure 7.

Figure 7 An example of type 1 variant: (a) original broken middle track, (b) linked middle alteration track

The last segment of the broken middle track in Figure 7(a) poses as a noise to a type 1 middle alteration track. Figure 7(b) shows the linked version of the broken segment. As a consequence, there is a failure in estimating CP. To overcome this situation, we deleted the last segment of the middle track before searching for type 1 and type 2 CPs.

If no CP can be obtained from both the original and the variant of type 1 and type 2 CP search, we concluded that the particular fingerprint directional field is either an arch or a tented arch which is of type 3. Figure 8 illustrates the initial condition for LCC, continuous initial condition for LCC, and the model of left and right alteration track for left and right AT.

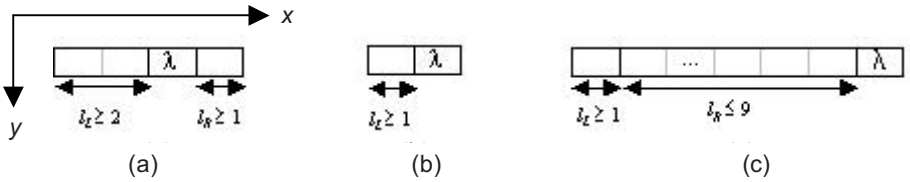

Figure 8 Left and right alteration tracking (a) initial condition for LCC, (b) continuous initial condition for LCC and (c) left and right alteration track model

Let λ pixel be a candidate pixel, l_L is the length of pixel *valuenL* which is to the left of the candidate pixel, and l_R is the length of pixel which is to the right of the candidate pixel. For left and right AT, λ in Figure 8(a) is a candidate pixel with grayscale value *valuenR*. A left alteration track records the transition from pixel value *valuenL* = 180 to pixel value *valuenR* = 144, whereas a right alteration track records the transition from pixel value *valuenL* = 108 to –33.75° pixel value *valuenR* = 72. The left alteration track is set to 144 and the right alteration track is set to 72. The continuous starting pixel is a valid tracking pixel if the absolute difference of the x-coordinate between the last

alteration track pixel and the continuous starting pixel is less than $M/3 - 1$. The value has been determined empirically.

LCC is the same as in Figure 6(c). By placing *p1, p2, p3, p4* or *p5* according to their priorities to λ in Figure 8(c), the selected pixel is a valid alteration track pixel if $l_L \geq 1$, and $l_R \leq 9$. As before, additional conditions are applied to *p1* and *p5*: *p1* must reside between regions with grayscale value $\geq valuenL$ at location $(x - 1, y - 1)$ and grayscale value $\leq valuenR$ at location $(x - 1, y + 1)$; whereas *p5* must reside between regions with grayscale value $\leq valuenR$ at location $(x + 1, y - 1)$ and grayscale value $\geq valuenL$ at location $(x + 1, y + 1)$.

An example is shown in Figure 9 where the longest track is the middle alteration track, the shortest track is the left alteration track, and the track on the right hand side of the middle alteration track is the right alteration track. The distance between the left track and right track is examined along the middle track. The point on middle alteration track that has smallest distance between the two tracks is decided as the true CP. True CPs marked by crosses on fingerprint directional fields are given in Figure 10.

Figure 9 Left, middle and right alteration track for type 3 middle alteration track

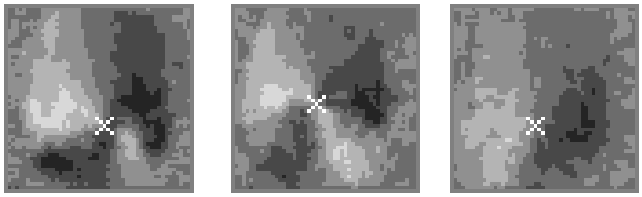

(a) (b) (c)

Figure 10 True centre points on directional fields (a) type 1, (b) type 2 and (c) type 3

4.0 FINGERPRINT FEATURE EXTRACTION

Fingerprint extraction process of fingerprint is based on the location of the CP on a fingerprint directional field to obtain a refined directional field. The located CP is positioned at the centre of the refined directional field in such a way that the refined fingerprint directional field is cropped until it is one-fourth of a fingerprint directional field, i.e. $N/16 \times N/16$ pixels. Three examples of fingerprint features (their corresponding true CPs are given in Figure 10) are illustrated in Figure 11.

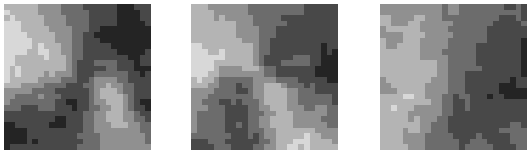

Figure 11 Examples of fingerprint features extracted from their respective original directional fields

5.0 PRINCIPAL COMPONENT ANALYSIS

Principal component analysis (PCA) method is adopted for classification of all aligned fingerprint features. PCA encodes information in a sense that information is compressed. Let X be a set of input images of J people, where each image is of dimension L, $X = \{x_1, x_2, x_3, ..., x_J\}$. Average image computed from the images is given by Equation (7):

$$\bar{x} = \frac{1}{J}\sum_{i=1}^{J} x_i \tag{7}$$

Sample mean is the difference from average image that input images are centred:

$$x_i^{'} = x_i - \bar{x} \tag{8}$$

Covariance matrix is given as the following:

$$C = \frac{1}{J}\sum_{i=1}^{J} x_i^{'} x_i^{'T} \tag{9}$$

Thus, eigenvalues and the corresponding eigenvectors can be obtained by solving:

$$Ce_i = \lambda_i e_i \tag{10}$$

Covariance matrix is of dimension $L \times L$. Eigenvalues $\lambda_1, \lambda_2, ..., \lambda_L$ are ranked in non-increasing order, corresponding to eigenvectors $e_1, e_2, ..., e_L$. For efficiency of the algorithm, only the eigenvectors corresponding to the top k eigenvalues are kept, forming the eigenspace. There are at most L-1 non-zero eigenvalues.

6.0 SIMILARITY MEASURES

To compare two projected vectors discussed in previous section, $\alpha = (\alpha_1, ..., \alpha_y)$ and $\beta = (\beta_1, ..., \beta_y)$, two popular similarity matching methods are employed viz the Euclidean distance (ED) and the Mahalanobis distance (MD). These are given as [7]:

ED:
$$d(\alpha, \beta) = \sqrt{\sum_{i=1}^{y} (\alpha_i - \beta_i)} \tag{11}$$

MD: $$d(\alpha,\beta) = d(\alpha-\beta)^T R^{-1}(\alpha-\beta) \quad (12)$$

where R is the decorrelation matrix.

7.0 EXPERIMENTAL RESULTS

This section provides analysis on the proposed fingerprint CP location algorithm and fingerprint verification system performance to highlight the feasibility of each of the proposed techniques at different stages of the conducted experiments.

7.1 Experimental Results for Fingerprint Centre Point Location

In our experiments, we evaluated two fingerprint databases, i.e. UTM_FING database (in-house fingerprint database) of size 416 × 416 captured from SAGEM MSO100 optical scanner and the database obtained from University of Bologna [8] which contains 168 images of size 256 × 256 from 21 fingers (8 items per finger). For experiments using UTM_ FING database, 386 images were randomly picked from 960 images. The CP location algorithm was tested on 386 images that obeyed the ROI. The first subtest was performed over the 386 images whereas the second subtest involved 381 fingerprints from all categories except 5 arch type fingerprints to compare the performance of the proposed algorithm with previous works.

From a total of 168 images of the Bologna database, 8 images were ignored due to poor quality fingerprint images, 3 images were exempted because their CPs were out of ROI, resulting in 157 images. The first subtest was performed over the 157 images and this subtest resulted in 7 failures where no CPs could be detected. Another subtest was done over 125 images, excluding 32 arch type fingerprint images and resulted in 5 failures.

Statistics of the successfully detected CP based on the four conducted experiments are tabulated in Table 2.

Table 2 Centre point location statistics

Test	No. of samples	Average distance from manually detected centre point (pixel)
UTM_FING database	386	2.36
UTM_FING database -without arch type images	381	2.25
Bologna database	150	4.36
Bologna database - without arch type images	120	3.89

Table 3 Comparison between the proposed algorithm and previous works

Test	Average distance from manually detected centre point (pixel)
Proposed algorithm	3.89
Algorithm from [4]	1.61
Algorithm from [2]	5.63

Statistical analysis of previous works is obtained from [4]. The average distances given are with respect to original image size. The CP location algorithm proposed in this work is with respect to $1/8 \times 1/8$ of original image size. To compare the proposed algorithm with previous works, the distances given in [4] are divided by 8. Comparisons between the proposed algorithm and previous works over all images of Bologna database except arch type images are given in Table 3. It can be seen from Table 3 that the performance of the proposed algorithm is between that of the other two previous algorithms.

7.2 Experimental Results for Fingerprint Verification

Two experiments have been carried out to evaluate the applicability of PCA algorithm in fingerprint verification paradigm utilizing the UTM_FING database. A total of 51 individuals were selected as a training set and 42 individuals from the remainders were impostors. We set that the located CPs should be no more than 5 pixels offset from the manually located CP. Three images per individual were randomly selected as training sample, whereas 2 images were taken for test images for genuine tests. A total of 2 test images were randomly selected from each impostor for impostor tests. The number of genuine tests and impostor tests performed were equal, which is 102.

The system is designed in such a way that if the similarity measured is less than a threshold, the test individual is accepted, or else the person is rejected. Different threshold values will result in different False Acceptance Rate (FAR) and False Rejection Rate (FRR). FAR is the probability that an impostor is accepted as an authorized user, whereas FRR is the probability that an authorized user is rejected mistakenly. Receiver Operating Characteristic (ROC) curves depicts the probability that an authorized user is accepted (100-FRR) against the probability that an impostor is accepted (FAR). The higher the rate of FAR and FRR, the worse is the accuracy. ROC curves corresponding to the 2 experiments are plotted in Figure 12 showing the performance of the verification algorithm. Both ED and MD give good performance for the proposed fingerprint verification system. Table 4 shows detailed analysis of both experiments for FAR fixed at 1.96%.

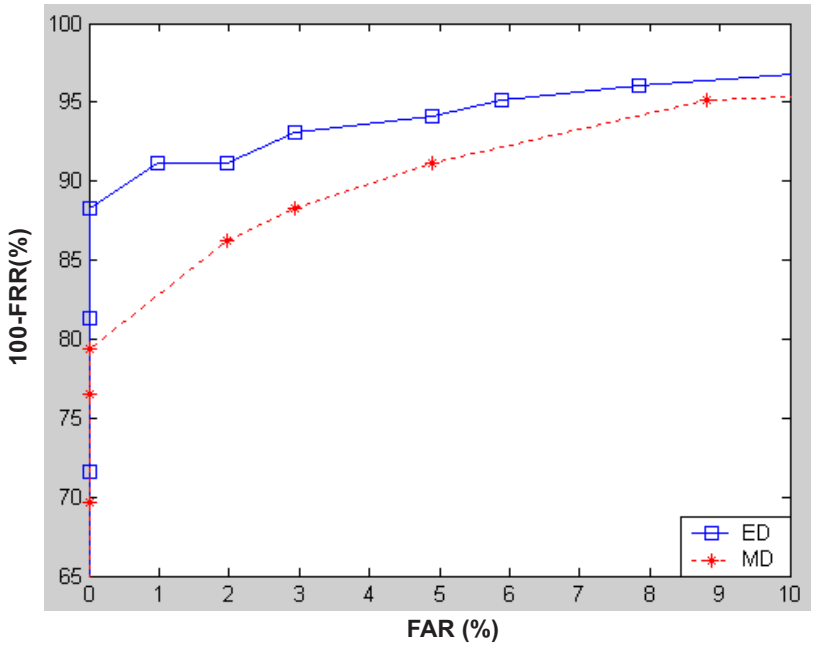

Figure 12 Receiver operating characteristic curves

Table 4 Comparison of eight experiments at FAR 1.96%

No.	Experiment	FRR (%)	Threshold	Accuracy (%)
1	ED	8.82	385	94.61
2	MD	13.73	35	92.16

8.0 CONCLUSIONS

In this paper, we present a fingerprint identity verification system by extracting fingerprint features based on fingerprint Centre Point (CP) location algorithm to increase the robustness of the system. CP locating is performed along the middle alteration track, thus having a fast access to locate the fingerprint CP as compared to performing search over the whole image. The proposed fingerprint CP location algorithm has been shown to give promising result, thus serves as a pre-processing for fingerprint verification. PCA algorithm is capable of dealing with extracted fingerprint features obtained from fingerprint directional field. Fingerprint directional field is utilized in CP location, feature extraction and fingerprint verification. From the experiments, the proposed system is able to achieve high accuracy.

REFERENCES

[1] Johan de Boer, A. M. Bazen, and S. H. Gerez. 2001. Indexing Fingerprint Databases Based on Multiple Features. Proc. ProRISC2001 Workshop on Circuit, Systems and Signal Processing. The Netherlands. 300-306.

[2] Jain, A. K., S. Prabhakar, H. Lin, and S. Pankanti. 2000. Filterbank-Based Fingerprint Matching. *IEEE Transactions on Image Processing*. 9: 846-859.

[3] Jain, A. K., S. Prabhakar, and H. Lin. 1999. A Multichannel Approach to Fingerprint Classification. *IEEE Transactions on Pattern Analysis and Machine Intelligence*. 21: 348-359.

[4] Kitiyanan, N., and J. P. Havlicek. 2004. Modulation Domain Reference Point Detection For Fingerprint Recognition. 6th IEEE Southwest Symposium on Image Analysis and Interpretation. Lake Tahoe, NV. March 28-30. 147-151.

[5] Bazen, A. M., and S. H. Gerez. 2002. Systematic Methods for the Computation of the Directional Fields and Singular Points of Fingerprints. *IEEE Transactions on Pattern Analysis and Machine Intelligence*. 24: 905-919.

[6] Mokji, M., and S. A. R. Abu-Bakar. 2004. Fingerprint Matching Based on Directional Image Constructed Using Expanded Haar Wavelet Transform. Proceedings of International Conference on Computer Graphics, Imaging and Visualization. Penang, Malaysia. 149-152.

[7] Navarrete, P., and Javier Ruiz-del-Solar. 2001. Eigenspace-based Recognition of Faces: Comparisons and a New Approach. Proceedings of the International Conference on Image Analysis and Processing ICIAP. Palermo, Italy. September 26-28. 42-47.

[8] Biometric System Lab (University of Bologna - ITALY): http://www.csr.unibo.it/research/biolab/